Modeling Magnetic Transport of Nanoparticles with Application to Magnetofection

E. P. Furlani and K. C. Ng
The Institute for Lasers, Photonics and Biophotonics, University at Buffalo SUNY
432 Natural Sciences Complex
Buffalo, NY 14260-3000
efurlani@buffalo.edu,

ABSTRACT

We present a model for predicting the transport and accumulation of magnetic nanoparticles in magnetophoretic systems. The model involves the solution of a drift-diffusion equation that governs the concentration of nanoparticles in a fluidic chamber. We solve this equation numerically using the finite volume method. We apply the model to the magnetofection process wherein the magnetic force produced by a rare-earth magnet attracts magnetic carrier particles with surface-bound gene vectors toward target cells for transfection. We study particle accumulation as a function of key variables.

Keywords: magnetofection, magnetic particle transport, drift-diffusion analysis, gene transfection, magnetic biotransport, magnetophoresis, gene delivery

1 INTRODUCTION

Magnetic nanoparticles are used in a broad range of bioapplications, primarily as carriers for biomaterials such as cells, proteins, antigens and DNA [1]. The use of biofunctional magnetic particles enables selective immobilization and transport of a biomaterial using an applied magnetic field. Moreover, magnetic biotransport enables accelerated delivery of biomaterial thereby overcoming diffusion-limited accumulation. This enables applications such as magnetofection, which involves the transfection of cells in a culture. In this process magnetic nanoparticles with surface-bound gene vectors are directed towards target cells using an applied magnetic field [2]. In a typical *in vitro* magnetofection system target cells are located at the bottom of a fluidic chamber (well of a culture plate), and a rare-earth magnet beneath the chamber provides a magnetic force that attracts the biofunctional particles towards the cells as shown in Fig. 1. The magnetic force accelerates the nanoparticle transport and enables rapid process times with significantly improved transfection rates.

In this paper we study the transport and accumulation of magnetic nanoparticles in a magnetophoretic system that consists of a fluidic chamber positioned above a cylindrical rare-earth magnet as shown in Fig. 1 We model particle transport using a drift-diffusion equation that governs the particle concentration within the chamber. We solve this equation numerically using the finite volume method (FVM), and we apply boundary conditions that mimic the magnetofection process. We use the model to study particle transport and accumulation. Our analysis indicates that the rate of accumulation at the base of thechamber can be controlled by choosing different sized particles and/or by adjusting the spacing between the magnet and the chamber. The model provides insight into the physics of particle transport and is useful for optimizing the performance of novel magnetofection systems.

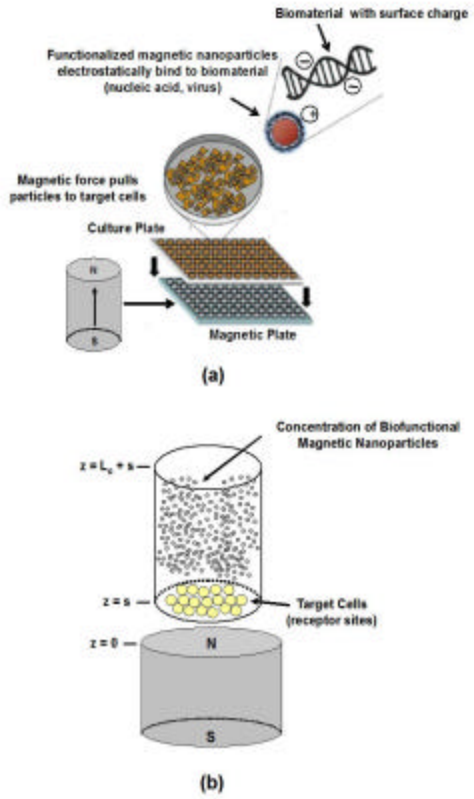

Figure 1: Magnetofection: (a) array of cell cultures positioned above an array of cylindrical rare-earth magnets (adapted from [6]), (b) the magnetic force pulls magnetic nanoparticles with surface bound gene vectors towards the cells.

2 THEORY

We model the transport of the nanoparticles using a drift-diffusion equation for the particle volume concentration $c(t)$ [3-4],

$$\frac{\partial c}{\partial t} = \nabla \bullet (\mathrm{D}\nabla c - \mathbf{U}c) \tag{1}$$

where $D = mkT$, $m = 1/(6\pi\eta R_{p,hyd})$ is the mobility of a particle with an effective hydrodynamic radius $R_{p,hyd}$, which takes into account surface-bound biomaterial, and η is the fluid viscosity. $\mathbf{U} = m\mathbf{F}$ is the drift velocity and $\mathbf{F}$ is the total force on the particle. In our analysis we take into account the fluidic $\mathbf{F}_\mathrm{f}$, magnetic $\mathbf{F}_\mathrm{m}$ and gravitational (buoyancy) $\mathbf{F}_g$ forces. We solve Eq. (1) numerically using the finite volume method (FVM). We use analytical expressions for the force components (drift velocity).

2.1 Magnetic Force

The magnetic force is given by

$$\mathbf{F}_\mathrm{m} = m_f \left(\mathbf{m}_\mathrm{p,eff} \bullet \nabla\right)\mathbf{H}_\mathrm{a} \tag{2}$$

where m_f is the permeability of the transport fluid, $\mathbf{m}_\mathrm{p,eff}$ is the "effective" dipole moment of the particle, and $\mathbf{H}_\mathrm{a}$ is the applied magnetic field intensity at the center of the particle. A model for $\mathbf{m}_\mathrm{p,eff}$ has been developed that takes into account self-demagnetization and magnetic saturation of the particle, i.e. $\mathbf{m}_\mathrm{p,eff} = \mathrm{V}_p f(\mathrm{H}_\mathrm{a})\mathbf{H}_\mathrm{a}$, where [4-8]

$$f(\mathrm{H}_\mathrm{a}) = \begin{cases} \dfrac{3(c_\mathrm{p} - c_\mathrm{f})}{(c_\mathrm{p} - c_\mathrm{f}) + 3} & \mathrm{H}_\mathrm{a} < \left(\dfrac{(c_\mathrm{p} - c_\mathrm{f}) + 3}{3c_\mathrm{p}}\right)\mathrm{M}_\mathrm{sp} \\ \mathrm{M}_\mathbf{sp} / \mathrm{H}_\mathrm{a} & \mathrm{H}_\mathrm{a} \geq \left(\dfrac{(c_\mathrm{p} - c_\mathrm{f}) + 3}{3c_\mathrm{p}}\right)\mathrm{M}_\mathrm{sp} \end{cases} \tag{3}$$

V_p is the volume of the particle, c_p and c_f are the magnetic susceptibilities of the particle and fluid, respectively, and $\mathrm{M}_\mathbf{sp}$ is the saturation magnetization of the particle.

2.2 Magnetic Field

We obtain an analytical expression for the field distribution by treating the magnet as an equivalent current source (section 3.3 of [9]). A cylindrical magnet that is uniformly magnetized along its axis produces the same field as a sheet of current that circulates around its circumference. We obtain the field distribution above the magnet by decomposing the "equivalent" current sheet into infinitesimal current loop elements and integrating the field contributions from the individual elements. The field solution for a current loop is well-known (p 263 in [10]). If the magnet is magnetized to saturation M_s, and centered about the z-axis with its top surface at $z = 0$ as shown in Fig. 1b, the applied field is given by

$$H_{ar}(r,z) = \frac{M_s}{2\pi}\int_{-L_m}^{0} \Pi_r(r,z)\,dz \qquad H_{az}(r,z) = \frac{M_s}{2\pi}\int_{-L_m}^{0} \Pi_z(r,z)\,dz, \tag{4}$$

where

$$\Pi_r(r,z) = \frac{z}{r\left((R_m + r)^2 + z^2\right)^{1/2}}\left[\frac{\left(R_m^2 + r^2 + z^2\right)}{\left((R_m - r)^2 + z^2\right)}E(k) - K(k)\right], \tag{5}$$

and

$$\Pi_z(r,z) = \frac{1}{r\left((R_m + r)^2 + z^2\right)^{1/2}}\left[\frac{\left(R_m^2 - r^2 + z^2\right)}{\left((R_m - r)^2 + z^2\right)}E(k) + K(k)\right], \tag{6}$$

In these expressions $K(k)$ and $E(k)$ are the complete elliptic integrals of the first and second kind, respectively, and $k^2 = \dfrac{4rR_m}{(R_m + r)^2 + z^2}$ where L_m and R_m are the length and radius of the magnet. We substitute Eqs. (4)-(6) into Eq. (2) and obtain an analytical expression for $\mathbf{F}_\mathrm{m}$, which is used in the numerical solution of Eq. (1).

3. MAGNETOFECTION

We use Eq. (1) to study the magnetofection process. Specifically, we predict the accumulation of magnetite (Fe_3O_4) nanoparticles at the base of a cylindrical fluidic chamber positioned above a rare-earth NdFeB magnet. The chamber has a radius R_c = 2 mm and length L_c = 3 mm, and is positioned 1 mm above the magnet, which has a radius R_m = 2.5 mm. length L_m = 5 mm, and is magnetized to saturation, $M_s = 8\times10^5$ A/m. The dimensions and parameters above are representative of a standard 96 well culture plate system that is used for magnetofection. We assume that the fluid in the chamber is nonmagnetic ($c_\mathrm{f} = 0$) with a viscosity and density equal to that of water, $\eta = 0.001$ N·s/m^2, and $\rho_f = 1000$ kg/m^3. Fe_3O_4 nanoparticles have a density $\rho_p = 5000$ kg/m^3 and a saturation magnetization $\mathrm{M}_{sp} = 4.78\times10^5$ A/m. Without loss of generality, we assume that the hydrodynamic radius of a particle is the same as its physical radius $R_{p,hyd} = R_p$.

We solve Eq. (1) subject to an initial condition in which there is a uniform particle concentration throughout the chamber. We apply a zero-flux Neumann boundary condition at the top of the chamber and a Dirichlet condition at the bottom. The latter condition mimics the magnetofection process wherein nanoparticles that reach the bottom of the chamber are removed from the

computation as it is assumed that they bind with receptor sites on target cells, and therefore no longer influence particle transport. It is assumed that there are a sufficient number of receptors to accommodate all of the particles in the chamber. We compute particle accumulation by summing the number of particles that reach the base of the chamber during each time step.

In our first study, we fix the particle radius R_p = 50 nm and compute particle accumulation, with and without a magnetic field (Fig. 2a). The analysis indicates that the rate of magnetically induced accumulation is orders of magnitude faster than that of diffusion-limited (no field) accumulation, which is consistent with experimental data shown in Fig. 2b [11]. We have performed similar calculations using a series of magnet to chamber spacings, and have found that the rate of accumulation increases substantially with decreasing separation.

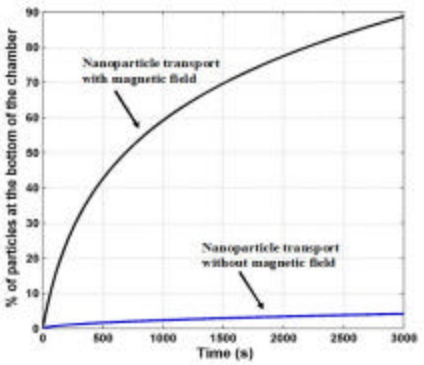

Figure 2: Nanoparticle accumulation: (a) predicted % of particles at the base of the chamber, (b) measured relative transfection efficiency, with and without an applied field (adapted from [11]).

Next, we compute the distribution of accumulated particles at the base of the chamber. We set R_p = 100 nm. The radial distribution of accumulated particles represented in terms of the particle volume concentration per unit area at the base of the chamber is shown in Fig. 3. Note that a higher concentration of particles occurs near the z-axis (centerline) above the magnet. This is due to the magnetic focusing of the particles during transport. There is also a local maximum in the concentration in an annulus around the centerline, which is due to the off-axis peaks in the axial force F_{mz} near the magnet. In summary, the magnetic particles accumulate towards the center of the chamber away from the edge of the magnet, where they are repelled inward by the magnetic force. This implies that higher transfection efficiencies would be achieved when the fluidic chamber has a smaller radius than the magnet.

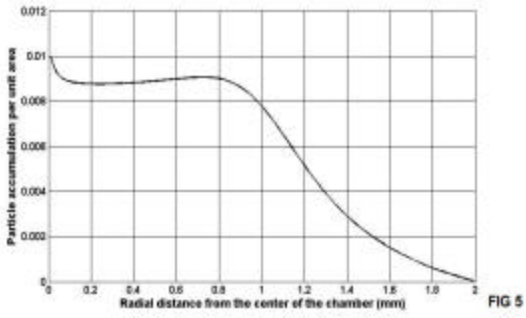

Figure 3: Distribution of particle accumulation per unit area at the base of chamber.

4 PARTICLE SATURATION

The drift-diffusion equation (1) does not account for particle volume saturation, i.e. it does not limit the number of particles that can physically occupy a given volume at a given time. We have developed a numerical method for addressing this issue, and have adapted it to the FVM. In the FVM the physical domain is discretized into a system of computational cells with each cell centered on a computational node. In 1D, the FVM discretization of Eq. (1) at an interior node is

$$c_i^{n+1} = c_i^n + \frac{dt}{dz}(F_{i+1/2} - F_{i-1/2}) \quad (i = 1,2,..., N_z) \tag{7}$$

where $dz = L_c / N_z$ is the length of a computational cell and L_c is the length of the chamber. c_i^n and c_i^{n+1} are the values of the concentration at the i'th computational node at time steps n and n+1, respectively. $F_{i\pm1/2}$ is a discretized version of the particle flux $D\frac{\partial c}{\partial z} - Uc$ at the edges of the computational cell $z_{i\pm1/2}$. As noted, we need to solve Eq. (7) taking into account particle accumulation/saturation, as each computational cell can only hold a finite number of finite-sized nanoparticles. We apply a two-step algorithm to account for. In the first step, we choose an initial time increment $dt_{initial}$ and use this in Eq. (7) to compute a temporary concentration at each computational node, i.e.,

$$c_{itemp}^{n+1} = c_i^n + \frac{dt_{initial}}{dz}(F_{i+1/2} - F_{i-1/2}) \quad (i = 1,2,..., N) \tag{8}$$

Next, we check to see if any of the c_{itemp}^{n+1} values are greater than the saturation concentration, which we denote by c_{sat}. If so, we identify the largest such temporary value and denote its index by $i_{\max}$, and its value by $\max(c_{itemp}^{n+1})$. We use this maximum value to compute a new global time increment dt_{new},

$$dt_{new} = \left(\frac{c_{sat} - c_i^n}{\max(c_{itemp}^{n+1}) - c_i^n} \right) dt_{initial} \tag{9}$$

In the second step of the algorithm, we recompute the concentration at each computational node using dt_{new} (i.e., substitute dt_{new} for $t_{initial}$ in Eq. (8)). It follows that $c_{i_{\max}}^{n+1} = c_{sat}$, and once a node is saturated we set the particle flux through its boundaries to zero for all subsequent times i.e. $c_i^{n+1} = c_{sat} \Rightarrow F_{i\pm 1/2} = 0$. The same algorithm can be used for 2D and 3D drift/diffusion analysis. Figure 4 illustrates a 1D implementations of the algorithm showing computational grids with regions of particle saturation. In this figure, a permanent magnet provides a magnetic force that moves the nanoparticles from left to right, producing regions of saturation on the right-hand-side of the computational domain. All boundaries are walled, i.e. zero flux. A 1D simulation showing particle accumulation is

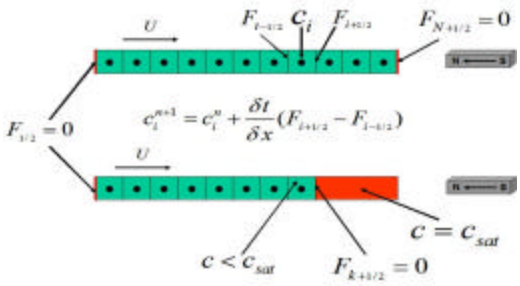

Figure 4: 1D FVM with particle saturation.

shown in Fig. 5. In this analysis the particles are initially distributed in the left half of the computational domain, which has closed (zero-flux) boundaries, and the magnetic force attracts particles from left to right.

5 CONCLUSIONS

Magnetic nanoparticles are increasingly used in bioapplications for the controlled transport of biomaterials. We have presented a model for predicting the transport and accumulation of such particles, and we applied it to the magnetofection process. We have found that magnetically-induced particle transport enables accumulation that is orders of magnitude faster than diffusion-limited accumulation, which is consistent with experimental observations. The model presented here provides a fundamental understanding of magnetophoresis at the nanoscale and enables optimization of novel magnetofection systems.

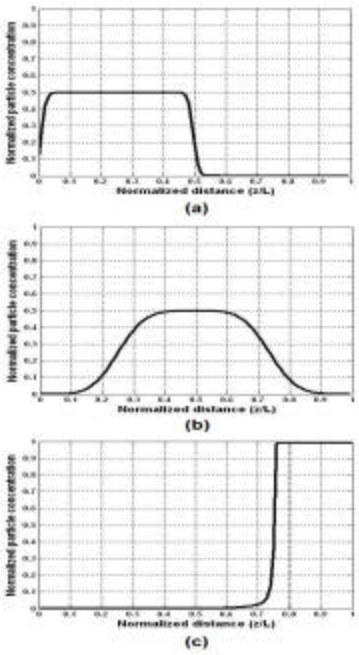

Figure 5: 1D particle concentration distribution analysis : (a) initial distribution, (b) intermediate distribution, (c) final distribution showing volume saturation.

REFERENCES

[1] Q. A. Pankhurst, J. Connolly, S.K. Jones, and J. Dobson, J. Phys. D: Appl. Phys. **36**, R167, 2003.

[2] U. Schillinger, T. Brilla, C. Rudolph, S. Huth, S. Gersting, F. Krötz, J. Hirschberger, C. Bergemann and C. Plank, J. Magn. Magn. Mat. **293**, 501, 200.

[3] D. Fletcher, IEEE Trans. Magn. **27** (4) 3655, 1991.

[4 E. P. Furlani, J. Appl. Phys. **99**, (2) 024912, 2006..

[5] E. P. Furlani and K. C. Ng, Phys. Rev. E **73**, 061919, 2006.

[6] E. P. Furlani and Y. Sahoo, J. Phys. D: Appl. Phys. **39**, 1724, 2006.

[7] E. P. Furlani and Y. Sahoo, J. Phys. D: Appl. Phys. **39**, 1724, 2006.

[8] E. J. Furlani and E. P. Furlani, J. Magn Magn. Mat. **312** (1), 187, 2007.

[9] E. P. Furlani, Permanent Magnet and Electromechanical Devices; Materials, Analysis and Applications, Academic Press, NY, 2001.

[10] J. A. Stratton, Electromagnetic Theory, McGraw-Hill, NY, 1941.

[11] C. Plank, F. Scherer, U. Schillinger, M. Anton and C. Bergemann, European Cells Mat. **3**, (Suppl. 2) 79-80, 2002.